Modeling and Simulation of a Silicon Beam Resonator Attached to a Square Diaphragm

Shangchun Fan,* Guangyu Liu, Man Hyung Lee*** and Kang Sup Yoon******

(*Received September 11, 1996*)

Based on the Finite Element Method (FEM) model of a practical silicon beam resonator attached to a square diaphragm used for measuring pressure, this paper presents two location error models which exist in actual fabrication. We calculate, analyze and investigate the relationship between the basic natural frequency of the beam resonator and the measured pressure for two error models by making use of FEM. In order to improve the exchangeability of the sensor, it is necessary to monitor the processing accuracy in x-and y-axes, and the reference angle relative to the ideal location within the positive stress range. It is also necessary to monitor the processing accuracy in the x-axis within the negative stress range, as the beam axial direction is along the x-asis the square diaphragm.

Key Words: Beam, Square Diaphragm, Pressure, Finite Element Method

Nomenclature

A,H	: Half length and thickness of the square diaphragm
X,Y	: Cartesian coordinate of the square diaphragm
P	: Pressure
A_0,A_0+L	: Axial coordinates of the beam in Cartesian coordinate of the square diaphragm
L,b,h	: Length, width and thickness of the beam which is attached to the square diaphragm
$-a,a$	: The local coordinates of the beam in Cartesian coordinate of the beam
B,D	: x-axis and y-axis deviations of the beam relative to its ideal location
α[deg.]	: The angular deviation of the beam relative to its ideal location
$W(x,y)$	: Displacement of the square diaphragm under the applied pressure P
Ds	: The flexural rigidity of the square diaphragm
E,ρ,μ	: Young modulus, density and poisson ratio of the sensing structure
$W_{\max}$	: Ratio between the maximum normal displacement and the thickness of the square diaphragm.
$\sigma_x(x,y),\sigma_y(x,y)$	: Stresses of the square diaphragm
$u(s,z,t),w(s,t)$	: Axial and normal vibrating displacements of the beam in Cartesian coordinate of the beam
t	: Time
s,z	: Axial and normal coordinates of the beam in Cartesian coordinate of the beam
$\sigma_s^0(s)$	: Initial axial stress of the beam
S	: Integrated length of the beam

* Professor, Department of Control Engineering, Beijing University of Aeronautics and Astronautics, Beijing, 100083, China
** Professor, Department of Control Engineering, Beijing University of Aeronautics and Astronautics, Beijing, 100083, China
*** Professor, Department of Control and Mechanical Engineering & ERC/Net Shape & Die Manufacturing, Pusan National University, Pusan, 609-735, Korea
**** Research Institute of Mechanical Technology, Pusan National University, Pusan, 609-735, Korea

$\omega[rad/s], w(s)$: Natural frequency and its corresponding vibrating shape along the axial direction of the beam
U : Potential energy of the beam
T : Kinetic energy of the beam
U_0 : Initial potential energy of the beam, which is caused by $\sigma_s^0(s)$
U_T : Total potential energy of the beam
S_j, S_{j+1} The jth and the (j+1)th node of the beam element
N : Total number of the beam element
q : Dimentionless variable in domain $s \in [S_j, S_{j+1}]$
l : Half length of the beam element in domain $s \in [S_j, S_{j+1}]$
$w_j(s), w_j(q)$: Displacement of the beam element in domain $s \in [S_j, S_{j+1}]$
$\mathbf{Q}_2^0$: The second order Hermite interpolation vector $[1 \quad q \quad q^2 \quad qs \quad q^4 \quad q^5]$
$\mathbf{G}_2$: The second order Hermite interpolation matrix
$\mathbf{a}_j$: Element nodal displacement vector $[w(-1) \quad w(-1)' \quad w''(-1) \quad w(+1) \quad w'(+1) \quad w''(+1)]^T$
U^j : Potential energy of the beam element in domain $s \in [S_j, S_{j+1}]$
T^j : Kinetic energy of the beam element in domain $s \in [S_j, S_{j+1}]$
U_0^j : Initial potential energy of the beam element in domain $s \in [S_j, S_{j+1}]$
U_T^j : Total potential energy of the beam element in domain $s \in [S_j, S_{j+1}]$
$\mathbf{K}^j$: The beam element stiffness matrix
$\mathbf{M}^j$: The beam element mass matrix
$\mathbf{K}_0^j$: The beam element initial stiffness matrix
$\mathbf{K}_T^j$: The beam element total stiffness matrix
$\mathbf{K}$: The assembly stiffness matrix
$\mathbf{M}$: The assembly mass matrix
$\mathbf{a}$: The assembly nodal displacement vector
$f(P,B,D,\alpha)[Hz]$: Basic natural frequency of the beam for pressure P, with x-axis deviation B, y-axis deviation D and the angular deviation α relative to its ideal location
$\Delta f(B,D,\alpha)[Hz]$: Variation of the basic natural frequency of the beam within (0, P), with x-axis deviation B, y-axis deviation D and the angular deviation α relative to its ideal location
$\beta(B,D,\alpha)$: Relative variation of the basic natural frequency variation of the beam within (0, P), with x-axis deviation B, y-axis deviation D and the angular deviation α relative to its ideal location

Superscripts

j : Number of the element
T : Transpose of matrix

Subscripts

j : Number of the element
T : Total
FEM : Finite element method result

1. Introduction

Resench and development on silicon resonant sensors has grown rapidly in recent years (Beeby, et al. 1995; Luo, 1996; Parsons, et al., 1992; Tilmans, et al. 1994). Silicon resonant sensors have advantages such as direct digital output (without A/D), long term stability, low hysteresis and high repeatability canparerd to generalized resonant sensors (Hauptmann, 1991). The advantages of silicon sensors include excellent mechanical properties, high strength, freedom from mechanical hysteresis, ability to batch process and therefore make low -cost, and the compatibility of mechanical and electrical properties. In addition, the temperature feature of silicon resonant sensors is much better than that of piezoresistive sensors. It is also much easier to interface with a microprocessor in order to develop smart

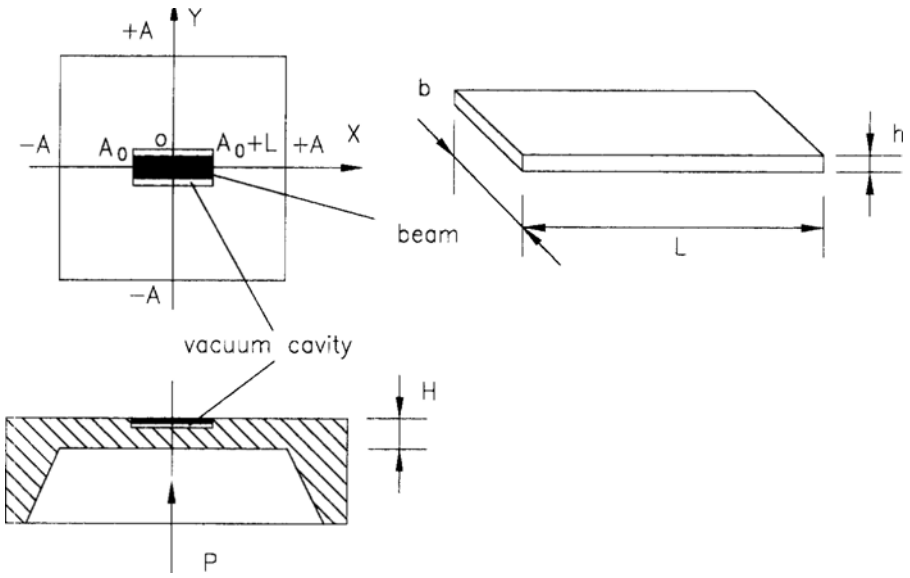

Fig. 1 Sensing structure of the sensor.

or intelligent sensors or sensor systems, due to its unique operating principle based on the relationship between the natural frequency and measured parameters such as pressure, force etc.

Figure. 1 shows the structure of a silicon resonant sensor for measuring pressure. The preliminary sensing unit is a square diaphragm. The measured pressure acts perpendicularly to the lower surface of the diaphragm and yields the stress. The final sensing unit is a beam, which is attached to the upper surface of the diaphragm. Moreover, the thickness of the beam h should be much less than the thickness of the diaphragm H, and the width of the beam should be less than the half length of the diaphragm A. Based on the above structural feature, an appropriate initial stress is applied along the axial direction of the beam, which is almost identical with the stress of the square diaphragm at the same position. Thus the natural frequency of the beam is varied with the applied pressure which acts on the square diaphragm. Therefore, the pressure will be measured via the change in natural frequency of the beam. In addition, the beam resonator has a very high Q factor because it can be packaged within a vacuum housing.

Figure 2 shows the ideal location scheme of the beam. Two error cases exist during the actual

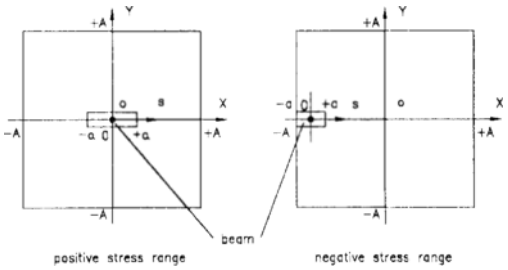

Fig. 2 Ideal locations of the beam at the diaphragm.

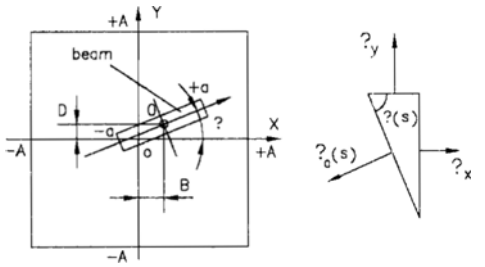

Fig. 3 Error model 1 of beam's location at the diaphragm.

fabrication. Figure 3 shows the location error model 1 within the positive stress range, while Figure 4 shows the location error model 2 within the negative stress range. It is certain that the frequency-pressure relationship varies with the deviation B in the x-axis, deviation D in the y-axis and the angular deviation α relative to its

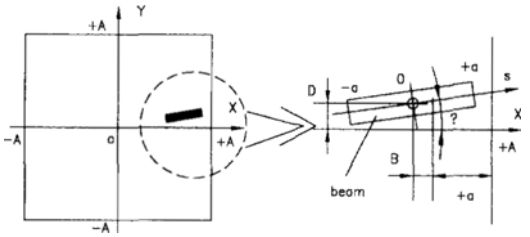

Fig. 4 Error model 2 of beam's location at the diaphragm.

ideal location for the above error cases. In order to improve the exchangeability of the sensor, it is necessary to investigate the influence laws of the above deviations on the frequency-pressure relationship of the beam resonator.

It is a typical mechanical problem for the vibration of a beam under a constant axial load. However, the silicon beam resonator, which is shown in Fig. 1, has never been discussed in the literature as far as we know until recenthy. The objective of this paper is to study the above problems in order to obtain some directions during developing and fabricating the silicon resonator sensors by making use of a finite element model (FEM).

2. Finite Element Modeling

2.1 Stresses on the upper surface of the square diaphragm

According to the structural feature and the design demands for the sensor, the square diaphragm is within the range of a small deflection. Then the differential equation can be written as follows (Timoshenko et al. 1959):

$$\frac{\partial^4 W(x,y)}{\partial x^4}+2\frac{\partial^4 W(x,y)}{\partial x^2\partial y^2}+\frac{\partial^4 W(x,y)}{\partial y^4}=\frac{P}{D_S} \tag{1}$$

where, $D_S=\dfrac{EH^3}{12(1-\mu^2)}$

According to the built-in edge of the square diaphragm, its displacement can be assumed as follows:

$$W(x,y)=W_{\max}H\left(\frac{x^2}{A^2}-1\right)^2\left(\frac{y^2}{A^2}-1\right)^2 \tag{2}$$

Substituting Eq. (2) into Eq. (1), the displacement $W(x,y)$ can be obtained. Then stresses on the upper surface of the square diaphragm can be obtained (Timoshenko et al. 1959):

$$\sigma_x(x,y)=-\frac{49P}{96}\left(\frac{A}{H}\right)^2\left[\left(\frac{3x^2}{A^2}-1\right)\left(\frac{y^2}{A^2}-1\right)^2+\mu\left(\frac{x^2}{A^2}-1\right)^2\left(\frac{3y^2}{A^2}-1\right)\right]$$

$$\sigma_y(x,y)=-\frac{49P}{96}\left(\frac{A}{H}\right)^2\left[\left(\frac{3y^2}{A^2}-1\right)\left(\frac{y^2}{A^2}-1\right)^2+\mu\left(\frac{y^2}{A^2}-1\right)^2\left(\frac{3x^2}{A^2}-1\right)\right] \tag{3}$$

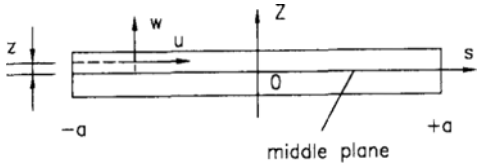

Fig. 5 Mathematical model of the beam.

2.2 Energy expressions of the beam

Figure 5 shows the mathematical model of the beam. The vibrating displacements of the beam at an arbitrary point are as follows:

$$\begin{cases} u(s,z,t)=-z\dfrac{dw(s)}{ds}\cos\omega t \\ w(s,t)=w(s)\cos\omega t \end{cases} \tag{4}$$

Energy expressions of the beam resonator are as follows (Rao, S. S., 1990):

The potential energy

$$U=\frac{Ebh^3\cos^2\omega t}{24}\int_S\left[\frac{d^2w(s)}{ds^2}\right]^2ds \tag{5}$$

The kinetic energy

$$T=\frac{\rho bh\omega^2\sin^2\omega t}{2}\int_S[w(s)]^2ds \tag{6}$$

In addition, the initial potential energy of the beam, which is caused by $\sigma_s^0(s)$, is

$$U_0=-\frac{bh\cos^2\omega t}{2}\int_S\sigma_s^0(s)\left[\frac{dw(s)}{ds}\right]^2ds \tag{7}$$

From Eq. (3) and Fig. 1, we have the following relation for the ideal case:

$$\sigma_s^0(s)=\sigma_x(x,0)=-\frac{49P}{96}\left(\frac{A}{H}\right)^2\left[\frac{3x^2}{A^2}-1\right)-\mu\left(\frac{x^2}{A^2}-1\right)^2\Big] \tag{8}$$

On the other hand, from Eq. Fig. 3 and Fig. 4, we have the following relation for the error cases (Timoshenko, et al. 1959):

$$\sigma_s^0(s) = \sin^2\beta(s)\,\sigma_x(x,y) + \cos^2\beta(s)\,\sigma_y(x,y) \tag{9}$$

$$\begin{cases} \sin^2\beta(s) = (A_0+0.5L+B+s\cos\alpha)^2 \Big/ \\ [A_0+0.5L+B+s\cos\alpha)^2+(D+s\sin\alpha)^2] \\ \cos^2\beta(s) = (D+s\sin\alpha)^2 / \\ (A_0+0.5L+B+s\cos\alpha)^2+(D+s\sin\alpha)^2] \end{cases}$$

Then the total potential energy of the beam is

$$U_T = U - U_0 \tag{10}$$

2.3 Finite element equation of the beam

In Eq. (7), if $\sigma_s^0(s)$ is a constant σ_s^0, the analytic relationship between the basic natural frequency and the initial axial stress can be directly obtained (Tilmans, et al. 1994):

$$\omega = \frac{4.73^2 h}{L^2}\left(\frac{E}{12\rho}\right)^{0.5}\left(1+0.295\frac{\sigma_s^0 L^2}{Eh^2}\right)^{0.5}[\mathrm{rad}/s] \tag{11}$$

However, from Eqs. (3), (8) and (9), $\sigma_s^0(s)$ is varying. Therefore, we present a finite element equation to solve the above problem.

Based on the above equations, we can divide the element along the axial direction of the beam, see Figure 6. Introducing the dimesionless length $q=(s-S_j)/l$, $l=0.5(S_{j+1}-S_j)$, the map of the domain $s\in[S_j,\ S_{j+1}]$ is $q\in[-1+1)$. For a displacement of the jth element, we introduce the second-order Hermite interpolation.

$$\begin{aligned} &w_j(s) = w_j(q) = \mathbf{Q}_2^0\mathbf{G}_2\mathbf{a}_j \\ &\mathbf{Q}_2^0 = [1\ \ q\ \ q^2\ \ q^3\ \ q^4\ \ q^5] \\ &\mathbf{a}_j = [w(-1)\ \ w'(-1)\ \ w''(-1)\ \ w(+2)\ \ w'(+1)\ \ w''(+1)]^T \end{aligned} \tag{12}$$

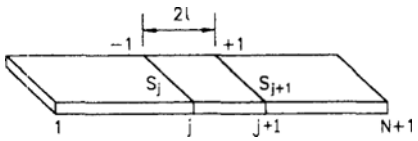

Fig. 6 Dividing element along beam's axial direction.

$$\mathbf{G}_2 = \frac{1}{16}\begin{bmatrix} 8 & 5l & l^2 & 8 & -5l & l^2 \\ -15 & -7l & -l^2 & 15 & -7l & l^2 \\ 0 & -6l & -2l^2 & 0 & 6l & -2l^2 \\ 10 & 10l & 2l^2 & -10 & 10l & -2l^2 \\ 0 & l & l^2 & 0 & -l & l^2 \\ -3 & -3l & -l^2 & 3 & -3l & l^2 \end{bmatrix}$$

From Eqs. (5) ~ (10), (12), we can obtain the element potential energy, kinetic energy, and initial potential energy in the domain $s\in[S_j, S_{j+1}]$. Then we can obtain the element stiffness matrix:

$$\mathbf{K}^j = \frac{Ebh^3}{12l^3}\int_{-1}^{+1}\mathbf{G}_2{}^T\mathbf{Q}_2^{2T}\mathbf{Q}_2^2\mathbf{G}_2\,dq \tag{13}$$
$$\mathbf{Q}_2^2 = \frac{d^2}{dq^2}\mathbf{Q}_2^0$$

The element mass matrix:

$$\mathbf{M}^j = \rho bhl\int_{-1}^{+1}\mathbf{G}_2{}^T\mathbf{Q}_2{}^{0T}\mathbf{Q}_2{}^0\mathbf{G}_2\,dq \tag{14}$$

The element initial stiffness matrix:

$$\begin{aligned} \mathbf{K}_0^j &= \frac{bh}{l}\int_{-1}^{+1}\sigma_s^0[S_j+(q+1)l] \\ &\quad \mathbf{G}_2{}^T\mathbf{Q}_2{}^{1T}\mathbf{Q}_2{}^1\mathbf{G}_2\,dq \\ \mathbf{Q}_2^1 &= \frac{d}{dq}\mathbf{Q}_2^0 \end{aligned} \tag{15}$$

The element total stiffness matrix:

$$\mathbf{K}_T^j = \mathbf{K}^j + \mathbf{K}_0{}^j \tag{16}$$

From Eqs. (16) and (14), the assembly stiffness matrix $\mathbf{K}$ and assembly mass matrix $\mathbf{M}$ can be obtained in the local domain $s\in[-a,\ +a]$. Then the finite element equation of the beam resonator can be written as follows:

$$(\mathbf{K}-\omega^2\mathbf{M})\mathbf{a} = 0 \tag{17}$$

where the assembly nodal vector $\mathbf{a}$ consists of all $\mathbf{a}_j$.

For the actual structural features of Fig. 1, the boundary conditions of the beam are as follows:

$$\begin{cases} s=-a: & w(s)=w'(s)=0 \\ s=+a: & w(s)=w(s)=0 \end{cases} \tag{18}$$

From Eqs. (17), (18), natural frequencies and the corresponding vibrating shapes of the beam resonator can be obtained.

4. Calculation and Discussion of Frequency Characteristics

Firstly, it is necessary to point out that the finite element solution of the first mode of Eq. (17) converges to the analytic solution of Eq. (11) as the element number N is more than 2, provided the the initial stress $\sigma_s^0(s)$ is a constant for the given parameters of the beam resonator. On the other hand, the solution of the first mode of Eq. (17) converges to a definite value as the element number N is more than 2, if the initial stress $\sigma_s^0(s)$ is in the form of Eq. (9). However, in this paper the element number N is selected to be 17 in order to investigate the detailed vibration shape of the beam resonator simultaneously.

The sensor is made of silicon, $E=1.3\times10^{11}\ pa$, $\rho=2.33\times10^3 kg/m^3$, $\mu=0.278$. The half length and thickness of the square diaphragm are $A=1\times10^{-3}\ m$ and $H=0.1\times10^{-3}m$, respectively. In addition, the width and thickness of the beam are $b=50\times10^{-6}m$ and $h=5\times10^{-6}m$.

Define $\Delta f(B, D, \alpha)[hz]=f(P, B, D, \alpha)-f(0, 0, 0, 0)$ as the variation of the basic natural frequency of the beam within $(0, P)$, with the x-axis deviation B, y-axis deviation D and the angular deviation α relative to its ideal location, where $f[Hz]=\omega[rad/s]/2\pi$.

Define $\beta(B, D, \alpha)=[\Delta f(B, D, \alpha)-\Delta f(0, 0, 0)]/\Delta f(0, 0, 0)$ as the relative variation of the basic natural frequency variation of the beam within $(0, P)$, with the x-axis deviation B, y-axis deviation D and the angular deviation α relative to its ideal location.

Table's 1~3 shows $\beta(B, D, 0)$, $(\alpha=0\text{deg})$, $\beta(B, D, 3)$ $(\alpha=+3\text{deg})$ and $\beta(B, D, -3)$ $(\alpha=-3\text{deg.})$, within $(0, 10^5)\ pa$, as the beam is located at different positions, i. e., with different x-axis deviation B, y-axis deviation D and the angular deviation α relative to its ideal location on the square diaphragm. The design ideal location is $(-300, +300)\times10^{-6}m$ (or $L=600\times10^{-6}m$) within the positive stress range of the beam, and the beam's axial direction is along the x-axis of the square diaphragm, which corresponds to $B=0$, $D=0$, $\alpha=0$. In addition, $f(0, 0, 0)=106648\ Hz$, $\Delta f(0, 0, 0)=9924 Hz$.

Table 1 The relative variation $\beta(B, D, 0)$ of the frequency variation of the beam.

	$B(\times10^{-6}m)$			
$D(\times10^{-6}m)$	0	2	4	6
0	0	0.001	0.001	0.001
2	0.002	0.001	0.001	0.001
4	0.001	0.001	0.001	0.001
6	0.001	0.001	0.001	0.001

Table 2 The relative variation $\beta(B, D, 3)$ of the frequency variation of the beam.

	$B(\times10^{-6}m)$			
$D(\times10^{-6}m)$	0	2	4	6
0	0	0.002	0.001	0.001
2	0.001	0.001	0.002	0
4	0.001	0.001	0.001	0.001
6	0.001	0.001	0.001	0.001

Table 3 The relative variation $\beta(B, D, -3)$ of the frequency variation of the beam.

	$B(\times10^{-6}m)$			
$D(\times10^{-6}m)$	0	2	4	6
0	0	0.002	0.001	0.001
2	0.001	0	0.001	0.001
4	0.001	0.002	0.002	0.001
6	0.002	0.001	0.002	0.001

From Table's 1~3, the variation of the basic natural frequency of the beam, which is influenced by the deviation D, the deviation B, and the angular deviation α of the beam relative to its ideal location, are almost the same within the positive stress range. Therefore, it is necessary to monitor the processing accuracy in x-axis, y-axis ,and the reference angle relative to the ideal coordinate during actual fabrication, in order to improve the exchangeability of the sensor.

Table's 4~6 show $\beta(B, D, 0)$ $(\alpha=0)$, $\beta(B, D, 3)$ $(\alpha=+3\text{deg.})$ and $\beta(B, D, -3)$ $(\alpha=-3\text{deg.})$, within $(0, 10^5)\ pa$, as the beam is located at different positions, i. e., with a different x-axis deviation B, y-axis deviation D, and the

Table 4 The relative variation $\beta(B,\ D,\ 0)$ of the frequency variation of the beam.

	$B(\times 10^{-6}m)$			
$D(\times 10^{-6}m)$	0	−2	−4	−6
0	0	−0.006	−0.020	−0.027
2	0	0.007	−0.020	−0.027
4	0.001	−0.007	−0.019	−0.028
6	0.003	−0.005	−0.017	−0.028

Table 5 The relative variation $\beta(B,\ D,\ 3)$ of the frequency variation of the beam.

	$B(\times 10^{-6}m)$			
$D(\times 10^{-6}m)$	0	−2	−4	−6
0	−0.001	−0.009	−0.024	−0.029
2	−0.002	−0.010	−0.023	−0.029
4	−0.002	−0.011	−0.021	−0.030
6	−0.004	−0.012	−0.026	−0.029

Table 6 The relative variation $\beta(B,\ D,\ -3)$ of the frequency variation of the beam.

	$B(\times 10^{-6}m)$			
$D(\times 10^{-6}m)$	0	−2	−4	−6
0	−0.001	−0.009	−0.024	−0.029
2	−0.001	−0.011	−0.025	−0.029
4	−0.003	−0.011	−0.022	−0.029
6	−0.002	−0.010	−0.018	−0.031

angular deviation α relative to its ideal location on the square diaphragm. The design ideal location is $(+700+1000)\times 10^{-6}$m (or $L=300\times 10^{-6}$ m) within the negative stress range of the beam, and the beam axial direction is along the x-axis of the square diaphragm, which corresponds to $B=0,\ D=0,\ \alpha=0$. In addition, $f(0,\ 0,\ 0,\ 0)=426564Hz,\ \Delta f(0,\ 0,\ 0)=10475Hz$.

From Table's 4~6, the variation of the basic natural frequency influenced by the deviation B is much greater than that influenced by the deviation D and the angular deviation α relative to its ideal location, within the negative stress range. Therefore, it is necessary to monitor the processing accuracy along the y-axis during actual fabrication within the negative range, i. e., the y-axis deviation B should be reduced as much as possible in order to improve the exchangeability of the sensor.

Compareing the above tables, it is obvious that locating the beam in the middle of the square diaphragm is much better than at the edge.

5. Conclusion

Based on the Finite Element Method model and analyses of the initial stresses applied to the beam resonator attached to a square diaphragm, this paper first calculates, analyzes and investigates the relationship between the basic natural frequency of the beam resonator and the measured pressure for two error models. An important result is obtained during the actual fabrication in order to improve the exchangeability of the sensor. That is: it is necessary to monitor the processing accuracy in the x-axis, y-axis and the reference angle α relative to the ideal coordinate, within the positive stress range, while only in the x-axis within the negative stress range as the beam axial direction is along the x-axis of the square diaphragm. In addition, locating the beam in the middle of the square diaphragm is much better than at the edge.

Acknowledgment

This work was supported by the Chinese Aeronautics Science Foundation, the Korea Science and Engineering Foundation, ERC/Net Shape & Die Manufacturing, and the Research Fund of the POSCO Chair Professor at Pusan National University.

References

Beeby, S. P. and Tudor, M. J., 1995, "Modeling and Optimization of Micromachined Silicon Resonators," *J. Micromech. Microeng.*, Vol. 5, pp. 103~105.

Hauptmann, P., 1991, "Resonant Sensors and Applications (Invited Paper)," *Sensors and Actuators*, Vol. A-27, pp. 371~377.

Luo, R. C., 1996, "Sensor Technologies and Microsensor Issues for Mechatronics Systems

(Invited Paper)," *IEEE/ASME Transactions on Mechatronics,* Vol. 1, pp. 39~49.

Parsons, P., Glendinning A. and Angelidis, D., 1992, "Resonator Sensor for High Accuracy Pressure Measurement Using Silicon Technology," Schlumberger Industries Aerospace, Transducer Division, *IEEE AES Magazine,* pp. 45~48.

Rao, S. S., 1990, *Mechanical Vibrations,* Addision-Wesley Publishing Company

Tilmans, H. A. C. and Legtenberg, R., 1994, "Electrostatically driven Vacuum-Encapsulated Polysilicon Resonators, Part two, Theory and Performance," Sensors and Actuators, A 45, pp. 67~84.

Timoshenko, S. P., Krieger S. W., 1959, *Theory of Plates and Shells,* McGraw-Hill Book Company, Inc.